Heat transfer in viscoplastic boundary layer flow from a vertical permeable cone with momentum and thermal wall slip : numerical study

Rao, AS, Prasad, VR, Radhika, VN and Beg, OA

http://dx.doi.org/10.1615/HeatTransRes.2017018153

HEAT TRANSFER RESEARCH-
AN OFFICIAL JOURNAL OF THE AMERICAN SOCIETY OF THERMAL AND FLUIDS ENGINEERS

Impact Factor= 0.930
ISSN: 1064-2285

Accepted October 26th 2016

HEAT TRANSFER IN VISCOPLASTIC BOUNDARY LAYER FLOW FROM A VERTICAL PERMEABLE CONE WITH MOMENTUM AND THERMAL WALL SLIP: *NUMERICAL STUDY*

A.SubbaRao[1*], V.R.Prasad[1], V. Naga Radhika[2] and **O. Anwar Bég[3]**

[1] *Department of Mathematics, Madanapalle Institute of Technology and Science, Madanapalle-517325,* ***India.***

[2] *Department of Mathematics, GITAM University Bangalore Campus, Bangalore -561203,* ***India.***

[3] *Fluid Mechanics, Aeronautical/Mechanical Engineering, Newton Building, University of Salford, Manchester M54WT,* ***UK.***

ABSTRACT

A mathematical model is presented for the laminar free convection boundary layer flow of Casson viscoplastic non-Newtonian fluid external to a vertical penetrable circular cone in the presence of thermal and hydrodynamic slip conditions. The cone surface is maintained at non-uniform surface temperature. The boundary layer conservation equations, which are parabolic in nature, are transformed into non-dimensional form via appropriate similarity variables, and the emerging boundary value problem is solved computationally with the second order accurate implicit Keller-box finite-difference scheme. The influence of velocity (momentum) slip, thermal slip and Casson non-Newtonian parameter on velocity, temperature, skin friction and Nusselt number are illustrated graphically. Validation of solutions with earlier published work is included. The computations show that the flow near the cone surface is strongly decelerated with increasing momentum slip whereas the temperature and thermal boundary layer thickness are increased. Increasing Casson parameter generally decelerates the flow and also decreases temperatures. Both velocity and thermal boundary layer thickness are reduced with greater Prandtl number. The study is relevant to petro-chemical engineering (polymer) processing systems.

Keywords: *Thermal convection; Slip condition; Keller-box numerical method; Skin friction; Nusselt number; Cone; Casson Viscoplastic model; Boundary layers; Buoyancy; Suction.*

**** Author for Correspondence;*** *Email- asrsvu@gmail.com*

Nomenclature:

C_f *skin friction coefficient*

S_f *non-dimensional momentum slip parameter*

S_T *non-dimensional thermal slip parameter*

f *non-dimensional stream function*

g *acceleration due to gravity*

V *transpiration velocity*

Gr *Grashof number*

N_0 *velocity slip factor*

K_0 *thermal slip factor*

Nu *local Nusselt number*

Pr *Prandtl number*

T *temperature*

u, v *non-dimensional velocity components along the x- and y- directions, respectively*

x, y *non-dimensional Cartesian coordinates along and transverse to cone surface*

Greek symbols

α *thermal diffusivity*

β *non-Newtonian Casson parameter*

Λ *coefficient of volume expansion*

Φ *azimuthal coordinate*

η *dimensionless radial coordinate*

μ *dynamic viscosity*

ν *kinematic viscosity*

θ *non-dimensional temperature*

ρ *density of fluid*

ξ *dimensionless tangential coordinate (free convection parameter)*

ψ *dimensionless stream function*

Subscripts

w *conditions on the wall*

∞ *free stream conditions*

1.INTRODUCTION

Many modern engineering applications involve the study of non-Newtonian fluids. These include petroleum drilling muds by Livescu [1], biological gels by Hron *et al.* [2], polymer processing by Loix *et al.* [3] and food processing by Kechichian *et al.* [4]. Most commonly, the viscosity of non-Newtonian fluids is dependent on *shear rate*. Some non-Newtonian fluids with shear-independent viscosity, however, still exhibit normal stress-differences or other non-Newtonian behaviour. Several salt solutions and molten polymers are non-Newtonian fluids, as are many other liquids encountered in science and technology such as dental creams, physiological fluids, detergents and paints. In a non-Newtonian fluid, the relation between the shear stress and the shear rate is generally non-linear and can even be time-dependent. The Casson model although simple is useful in simulating a number of polymers, for example alcoflood polymers employed in enhanced oil recovery by Ghannam and Esmail [5]. The Casson model was originally introduced to describe printing inks by Casson [6]. It is a *viscoplastic fluid model* which exhibits shear thinning characteristics, yield stress (below which no flow occurs) and high shear viscosity as elaborated by Bird *et al*. [7]. The Casson fluid model tends to a Newtonian fluid at a very high wall shear stress i.e. when the wall stress is far greater than yield stress. To improve processing of many types of polymers, numerous investigators have conducted simulations of Casson flow dynamics using many computational and analytical methods. These studies have included heat transfer (important for thermal treatment), mass transfer (critical to doping modification of polymers), viscous heating, magneto hydrodynamics (for electro-conductive polymers) and many other phenomena. Hayat *et al.* [8] used the homotopy analysis method to investigate the dissipative stagnation-point flow and heat transfer of a Casson fluid along a stretching surface. Nasir *et al.* [9] employed a perturbation technique to investigate combined heat, mass and momentum transfer in transient flow of Casson fluid between a long vertical wavy wall and a parallel wavy wall under convective boundary conditions. Reddy *et al.* [10] used both homotopy analysis and Adomian decomposition methods to simulate dissipative magnetized Casson fluid flow in a vertical conduit. Nagarani and Lewis [11] studied the transport of Casson liquids in an annular gap under peristaltic waves using lubrication theory. They observed that both yield stress and annular gap significantly influence pressure rise and frictional resistance on the walls. Pham and Mitsoulw [12] used a finite element method to simulate entry and exit Casson fluid flows through abrupt contractions, showing that the swelling ratio of the free stream for planar and axisymmetric contraction flows is very sensitive

to Casson viscoplastic parameter. Tripathi and Bég [13] utilized Mathematica symbolic software integration routines to investigate the peristaltic propulsion of Casson, Vocadlo and other viscoplastic fluids, showing that the yield stress model selected dramatically influences volumetric flow rates and wall shear stress. Xiang and Chen [14] utilized mesh free methods to study Poiseuille and other flows of both Casson and Cross non-Newtonian liquids. Shankran [15] used FLUENT computational fluid dynamics software to extensively visualize the flow of Casson fluids in corrugated channels. Mustafa *et al*. [16] employed a homotopy power series method to study dissipative boundary layer flow of a Casson fluid generated by an impulsively started moving sheet, noting that surface shear stress and heat transfer rate are respectively elevated and decreased with Casson fluid parameter. Batra and Das [17] obtained analytical solutions for time-dependent Casson fluid flow in the annular space between two coaxial rotating cylinders, evaluating in detail the influence of Casson parameter and aspect ratio on the extent of core formation. Very recently Akbar *et al.* [18] used integral methods to determine velocity and temperature distributions in hydro magnetic dissipative cilia-beat generated propulsion of Casson fluids in two-dimensional configurations

The previous studies invariably assumed the classical "no-slip" condition at the boundary. Slip effects have however shown to be important in numerous polymeric transport processes including the production stage of polymers from the raw (monomeric) materials and in converting high-molecular-weight products into specific products by W.B. Black [19]. Many researchers, primarily in chemical engineering have therefore studied, both experimentally and numerically, the influence of wall slip on polymer dynamics. Important works in this regard include Wang *et al.* [20] who considered low density polyethylene liquids, Piau *et al.* [21] who addressed polymer extrudates, Piau and Kissi [22] who quantified macroscopic wall slip in polymer melts, Lim and Schowalter [23] who studied boundary slip in polybutadiene flows and Hatzikiriakos and Kalogerakis [24] who also studied molten polymer wall slip. Wall slip in *thermal polymer processing* was considered by Liu and Gehde [25] in which slip was shown to significantly modify temperature distribution in polymers. Hatzikiriakos and Mitsoulis [26] presented closed-form solutions and finite element computations for wall slip effects on pressure drop of power-law fluids in tapered dies. Many studies of both momentum (hydrodynamic or velocity) slip and thermal slip on transport phenomena have also been reported. Sparrow *et al.* [27] presented the first significant analysis of laminar slip-flow heat transfer for tubes with uniform heat flux, observing that

momentum slip acts to improve heat transfer whereas thermal slip (or "temperature jump") reduces heat transfer. Subba Rao *et al.* [28] considered velocity on thermal slip effects on thermal convection boundary layer flow of Casson fluids with buoyancy effects. Uddin *et al.* [29] used Maple software to compute the influence of anisotropic momentum, thermal, and multiple species slip on three-dimensional stagnation point boundary layers in nanofluid bio-convection flows.

Heat transfer with and without slip in *external* boundary layers from *curved bodies* are also of interest in *polymeric enrobing systems*. Subba Rao *et al.* [30] studied numerically the combined effects of thermal and velocity slip and radiative flux on steady Casson enrobing boundary layer from a horizontal cylinder in porous media. They noted that greater velocity slip increases thermal boundary layer thickness and also momentum boundary layer thickness, whereas greater thermal slip decreases momentum boundary layer thickness (i.e. decelerates the flow) and cools the regime. Hering and Grosh [31] presented an early classical study on natural convection boundary layers non-isothermal cone, showing that similarity solutions exist when the wall temperature distribution is a power function of distance along a cone ray. They further documented solutions for an isothermal surface as well as for the surface maintained at the temperature varying linearly with the distance measured from the apex of the cone for Prandtl number of 0.7. Hering [32] re-visited the problem in Hering and Grosh [31] to consider low Prandtl number fluids (i.e. high thermal conductivity fluids such as liquid metals) for constant wall heat flux conditions. Further studies of heat transfer from conical bodies have been communicated by Alamgir [33] who used an integral method, Hossain and Paul [34] who considered surface blowing/suction effects and Chamkha [35] who studied the case of heat transfer from a truncated cone with magnetohydrodynamic and radiation flux effects. Bég *et al.* [36] used the network electro-thermal PSPICE code to elaborate the influence of buoyancy, wall mass flux, pressure work and dissipation on hydromagnetic convection from a non-isothermal cone. Saleem and Nadeem [37] used an optimized homotopy method to derive series solutions for thermal convection slip flow from a rotating one, observing that increasing hydrodynamic slip decelerates the primary flow nearer the cone surface, accelerates the primary flow further from the cone surface and consistently reduces secondary velocity. Very recently Bég *et al.* [38] presented novel solutions based on shooting quadrature for the heat transfer from a rotating cone in anisotropic porous media. Basir *et al.* [39] considered transient nanofluid bioconvection boundary layer flow from a stretching horizontal cylinder with four slip mechanisms- thermal, velocity, nano-particle mass and micro-organism slip. Several studies have

also utilized the Casson fluid in slip modelling. Prasad *et al.* [40] obtained finite difference solutions for nonlinear heat and momentum transfer from a sphere in Darcy-Forchheimer porous media with velocity and thermal slip effects. Subba Rao *et al.* [41] reported on multiple slip effects in Casson boundary layer convection from a sphere observing that both thermal and hydrodynamic slip significantly alter surface skin friction and Nusselt numbers.

In the present work, a mathematical model is developed for steady, natural convection boundary layer flow in a Casson viscoplastic polymeric fluid external to a vertical permeable circular cone maintained at non-uniform surface temperature. A finite difference numerical solution is obtained for the transformed nonlinear two-point boundary value problem subject to physically appropriate boundary conditions at the cone surface and in the free stream. The impact of the emerging thermo physical parameters i.e. Casson non-Newtonian parameter, momentum (velocity) slip, thermal slip and Prandtl number on velocity, temperature, wall shear stress function and Nusselt number, in the presence of wall suction, are presented graphically and in Tables. Validation with previous Newtonian studies is included. Detailed evaluation of the physics is included. The present problem has to the authors' knowledge not appeared thus far in the scientific literature and is relevant to thermal treatment of polymeric enrobing systems by Dealy and Wissbrun [42].

2. MATHEMATICAL THERMO-VISCOPLASTIC FLOW MODEL

Consider the steady, laminar, two-dimensional, viscous, incompressible, buoyancy-driven convection flow from a non-isothermal vertical porous cone embedded in a Casson non-Newtonian fluid. **Figure 1(a)** depicts the flow model and physical coordinate system.

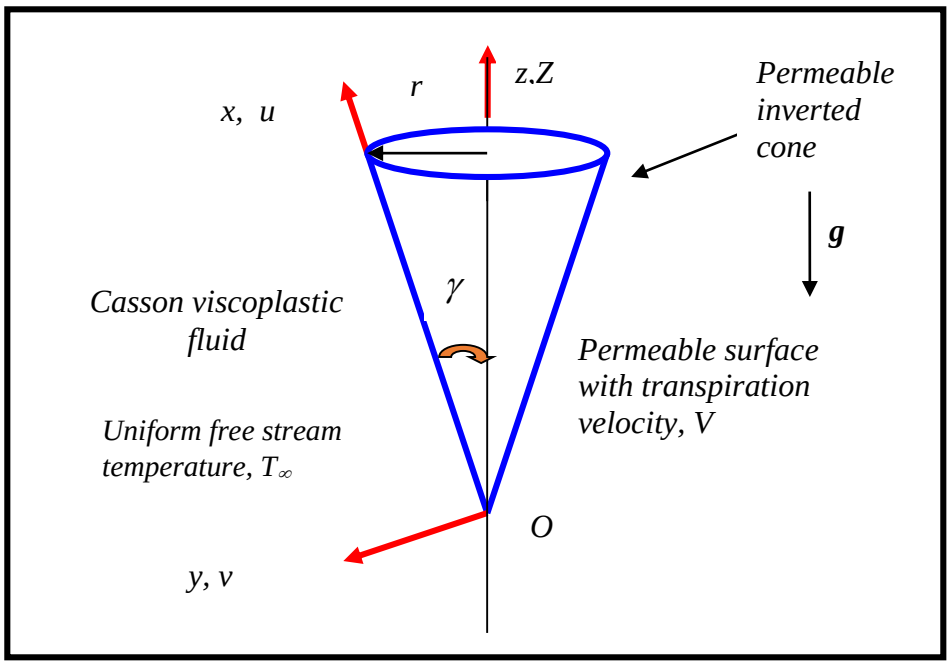

Fig. 1(a) Physical Model and Coordinate System

The *x*-coordinate is measured along the circumference of the circular cone from the cone apex (*O*) and the *y*-coordinate is measured normal to the surface. The gravitational acceleration, ***g*** acts downwards. Both the circular cone and the fluid are maintained initially at the same temperature. Instantaneously they are raised to a temperature $T_w > T_\infty$, in which T_w is the ambient temperature of the fluid which remains unchanged. The constitutive equation for an isotropic viscoplastic Casson fluid, following Bird *et al.* [7] in tensorial notation may be stated as:

$$\tau_{ij} = \begin{cases} 2\left(\mu_B + \dfrac{p_y}{\sqrt{2\pi}}\right)e_{ij}, \pi \geq \pi_c \\ 2\left(\mu_B + \dfrac{p_y}{\sqrt{2\pi_c}}\right)e_{ij}, \pi < \pi_c \end{cases} \tag{1}$$

Here all parameters are defined in the nomenclature. In line with the approach of Yih [43] and introducing the boundary layer approximations, the governing conservation equations can be written as follows:

$$\frac{\partial(ur)}{\partial x} + \frac{\partial(vr)}{\partial y} = 0 \tag{2}$$

$$u\frac{\partial u}{\partial x} + v\frac{\partial u}{\partial y} = g\Lambda(T - T_\infty)\cos\gamma + \nu\left(1 + \frac{1}{\beta}\right)\frac{\partial^2 u}{\partial y^2} \tag{3}$$

$$u\frac{\partial T}{\partial x}+v\frac{\partial T}{\partial y}=\alpha\frac{\partial^2 T}{\partial y^2} \tag{4}$$

where u and v are the velocity components in the x - and y - directions respectively, ν - the kinematic viscosity of the fluid, β - is the non-Newtonian Casson parameter, α - the thermal diffusivity, g - acceleration due to gravity, γ is the cone apex half- angle and T - the temperature of the fluid respectively. The boundary conditions are prescribed at the cone surface and the edge of the boundary layer regime (free stream), respectively as follows:

$$\text{At}\quad y=0,\qquad u=N_0\left(1+\frac{1}{\beta}\right)\frac{\partial u}{\partial y},\quad v=V_w,\ T=T_w+K_0\frac{\partial T}{\partial y} \tag{5}$$

$$\text{As}\quad y\to\infty,\qquad u\to 0,\ T\to T_\infty$$

Here V represent the transpiration velocity at the surface of the permeable cone. When V is positive, this represents uniform wall suction (or lateral mass flux withdrawal) and when V is negative, this corresponds to surface injection (or blowing) of fluid into the fluid body. In the present case, only suction is considered and therefore, V is taken as positive throughout. Furthermore, N_0 is the velocity slip factor and K_0 is the thermal slip factor. For $N_0=0=K_0$, one can recover the classical *no-slip* case. The stream function ψ is defined by $u=\frac{1}{r}\partial\psi/\partial y$ *and* $v=-\frac{1}{r}\partial\psi/\partial x$ and therefore, the continuity equation (2) is automatically satisfied. In order to write the governing equations and the boundary conditions in dimensionless form, the following non-dimensional quantities are introduced (as defined in the nomenclature).

$$\xi=\frac{Vx}{\nu}\sqrt[4]{Gr},\qquad \eta=\frac{y}{x}\sqrt[4]{Gr},\qquad \psi=\nu r\sqrt[4]{Gr}\left(f+\frac{1}{2}\xi\right),\qquad \Pr=\frac{\nu}{\alpha}$$

$$\theta(\xi,\eta)=\frac{T-T_\infty}{T_w-T_\infty},\quad Gr=\frac{g\Lambda\cos\gamma(T_w-T_\infty)x^3}{\nu^2},\quad \beta=\mu_B\frac{\sqrt{2\pi_c}}{p_y},\qquad r=x\sin\gamma \tag{6}$$

In view of Equation (6), Equations (2) - (4) reduce to the following coupled, nonlinear, dimensionless partial differential equations for momentum and heat (energy) conservation for the regime:

$$\left(1+\frac{1}{\beta}\right)f'''+\frac{7}{4}ff''-\frac{1}{2}f'^2+\theta=\frac{7}{4}\xi\left(f'\frac{\partial f'}{\partial\xi}-f''\frac{\partial f}{\partial\xi}\right) \tag{7}$$

$$\frac{\theta''}{\Pr}+\frac{7}{4}f\theta'=\frac{7}{4}\xi\left(f'\frac{\partial\theta}{\partial\xi}-\theta'\frac{\partial f}{\partial\xi}\right) \tag{8}$$

The transformed dimensionless boundary conditions are:

$$\text{At}\quad \eta=0,\quad f=f_w=S,\qquad f'=\left(1+\frac{1}{\beta}\right)S_f f''(0),\qquad \theta=1+S_T\theta'(0)$$

$$\text{As}\quad \eta\to\infty,\quad f'\to 0,\quad \theta\to 0 \tag{9}$$

In the above equations, the primes denote the differentiation with respect to η, the dimensionless radial coordinate, ξ is the dimensionless tangential coordinate, Φ - the azimuthal coordinate, *Gr* is the Grashof (free convection) parameter, $\Pr=\frac{\nu}{\alpha}$ the Prandtl number, $S_f=\frac{N_0 Gr^{1/4}}{x}$ and $S_T=\frac{K_0 Gr^{1/4}}{x}$ are the non-dimensional velocity slip and thermal slip parameters respectively and *S* is the suction (wall mass flux) parameter. Here we assumed the typical values $K_0 = 0.5$, $N_0 = 0.25$ for finding the non-dimensional velocity and thermal slip parameters.

The dimensionless local values of the skin-friction coefficient and the Nusselt number, may be defined as follows:

$$C_f Gr^{1/4}=\left(1+\frac{1}{\beta}\right)f''(0) \tag{10}$$

$$\frac{Nu}{\sqrt[4]{Gr}}=-\theta'(0) \tag{11}$$

3. NUMERICAL SOLUTIONS WITH KELLER BOX SCHEME

The coupled boundary layer equations in a (ξ,η) coordinate system remain strongly nonlinear. A numerical method, the Keller-Box implicit difference method, is therefore deployed to solve the boundary value problem defined by Ens. (7)-(8) with boundary conditions (9). This technique has been described succinctly in Cebeci and Bradshaw [44] and Keller [45]. It has been used recently in polymeric flow dynamics by Subba Rao *et al*. [46] for viscoelastic models and Prasad *et al*. [47] for micropolar liquids. The key stages involved are as follows:

a. Reduction of the N^{th} order partial differential equation system to *N* first order equations
b. Finite difference discretization
c. Quasilinearization of non-linear Keller algebraic equations
d. Block-tridiagonal elimination of linear Keller algebraic equations

Phase a: ***Reduction of the N^{th} order partial differential equation system to N first order equations***

Equations (7)-(8) subject to the boundary conditions (9) are first written as a system of first-order equations. For this purpose, we reset Eqns. (7) – (8) as a set of simultaneous equations by introducing the new variables *u, v* and *t*:

$$f' = u \tag{12}$$

$$f'' = v \tag{13}$$

$$\theta' = t \tag{14}$$

$$\left(1+\frac{1}{\beta}\right)v' + \frac{7}{4} fv - \frac{1}{2}u^2 + s = \frac{7}{4}\xi\left(u\frac{\partial u}{\partial \xi} - v\frac{\partial f}{\partial \xi}\right) \tag{15}$$

$$\frac{1}{\mathrm{Pr}}t' + \frac{7}{4} ft = \frac{7}{4}\xi\left(u\frac{\partial s}{\partial \xi} - t\frac{\partial f}{\partial \xi}\right) \tag{16}$$

where primes denote differentiation with respect to η.

In terms of the dependent variables, the boundary conditions become:

$$\begin{aligned} &At \qquad \eta = 0: \quad u = \left(1+\frac{1}{\beta}\right) f''(0), \quad f = S, \quad s = 1 \\ &As \qquad \eta \to \infty: \quad u \to 0, \quad s \to 0 \end{aligned} \tag{17}$$

Phase b: ***Finite Difference Discretization***

A two dimensional computational grid is imposed on the ξ-η plane as sketched in **Fig. 1(b).** The stepping process is defined by:

$$\eta_0 = 0, \qquad \eta_j = \eta_{j-1} + h_j, \quad j = 1, 2, ..., J, \qquad \eta_J \equiv \eta_\infty \tag{18}$$

$$\xi^0 = 0, \qquad \xi^n = \xi^{n-1} + k_n, \quad n = 1, 2, ..., N \tag{19}$$

where k_n and h_j denote the step distances in the ξ and η directions respectively.

If g_j^n denotes the value of any variable at $\left(\eta_j, \xi^n\right)$, then the variables and derivatives of Equations. (12) – (16) at $\left(\eta_{j-1/2}, \xi^{n-1/2}\right)$ are replaced by:

$$g_{j-1/2}^{n-1/2} = \frac{1}{4}\left(g_j^n + g_{j-1}^n + g_j^{n-1} + g_{j-1}^{n-1}\right), \tag{20}$$

$$\left(\frac{\partial g}{\partial \eta}\right)_{j-1/2}^{n-1/2} = \frac{1}{2h_j}\left(g_j^n - g_{j-1}^n + g_j^{n-1} - g_{j-1}^{n-1}\right), \tag{21}$$

$$\left(\frac{\partial g}{\partial \xi}\right)_{j-1/2}^{n-1/2} = \frac{1}{2k^n}\left(g_j^n - g_{j-1}^n + g_j^{n-1} - g_{j-1}^{n-1}\right), \tag{22}$$

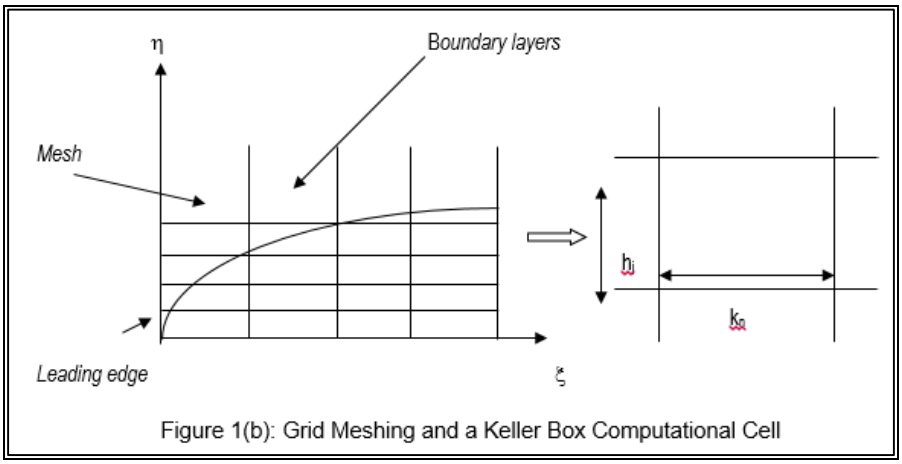

Figure 1(b): Grid Meshing and a Keller Box Computational Cell

We now formulate the finite-difference approximation of equations. (12) – (16) for the mid-point $\left(\eta_{j-1/2}, \xi^n\right)$, below

$$h_j^{-1}\left(f_j^n - f_{j-1}^n\right) = u_{j-1/2}^n, \tag{23}$$

$$h_j^{-1}\left(u_j^n - u_{j-1}^n\right) = v_{j-1/2}^n, \tag{24}$$

$$\begin{aligned}\left(1+\frac{1}{\beta}\right)\left(v_j - v_{j-1}\right) + \frac{7h_j(1+\alpha)}{16}\left[\left(f_j + f_{j-1}\right)\left(v_j + v_{j-1}\right)\right] - \frac{h_j}{16}(2+7\alpha)\left(u_j + u_{j-1}\right)^2 \\ + \frac{7h_j\alpha}{8}v_{j-1/2}^{n-1}\left(f_j + f_{j-1}\right) - \frac{7\alpha h_j}{8}f_{j-1/2}^{n-1}\left(v_j + v_{j-1}\right) + \frac{h_j}{2}\left(s_j + s_{j-1}\right) = \left[R_1\right]_{j-1/2}^{n-1}\end{aligned} \tag{25}$$

$$h_j^{-1}\left(\theta_j^n - \theta_{j-1}^n\right) = t_{j-1/2}^n \tag{26}$$

$$\frac{1}{\Pr}\left(t_j - t_{j-1}\right) + \frac{7\left(1+\alpha\right)h_j}{16}\left[\left(f_j + f_{j-1}\right)\left(t_j + t_{j-1}\right)\right] - \frac{7\alpha h_j}{16}\left[\left(u_j + u_{j-1}\right)\left(s_j + s_{j-1}\right)\right]$$
$$+ \frac{7\alpha h_j}{8} s_{j-1/2}^{n-1}\left(u_j + u_{j-1}\right) - \frac{7\alpha h_j}{8} u_{j-1/2}^{n-1}\left(s_j + s_{j-1}\right) - \frac{7\alpha h_j}{8} f_{j-1/2}^{n-1}\left(t_j + t_{j-1}\right) \tag{27}$$
$$+ \frac{7\alpha h_j}{8} t_{j-1/2}^{n-1}\left(f_j + f_{j-1}\right) = \left[R_2\right]_{j-1/2}^{n-1}$$

Here we have used the abbreviations

$$\alpha = \frac{\xi^{n-1/2}}{k_n} \tag{28}$$

$$\left[R_1\right]_{j-1/2}^{n-1} = -h_j\left[\left(1+\frac{1}{\beta}\right)\left(\frac{v_j - v_{j-1}}{h_j}\right) + \frac{7}{4}\left(1-\alpha\right)\left(f_{j-1/2}v_{j-1/2}\right) + \left(\frac{7\alpha-2}{4}\right)\left(u_{j-1/2}\right)^2 + \left(s_{j-1/2}\right)\right] \tag{29}$$

$$\left[R_2\right]_{j-1/2}^{n-1} = -h_j\left[\frac{1}{\Pr}\left(\frac{t_j - t_{j-1}}{h_j}\right) + \frac{7}{4}\left(1-\alpha\right)\left(f_{j-1/2}t_{j-1/2}\right) + \frac{7}{4}\alpha\left(u_{j-1/2}s_{j-1/2}\right)\right] \tag{30}$$

The boundary conditions are

$$f_0^n = u_0^n = 0, \qquad \theta_0^n = 1, \qquad u_J^n = 0, \qquad \theta_J^n = 0 \tag{31}$$

Phase c: ***Quasilinearization of Non-Linear Keller Algebraic Equations***

If we assume $f_j^{n-1}, u_j^{n-1}, v_j^{n-1}, s_j^{n-1}, t_j^{n-1}$ to be known for $0 \le j \le J$, Equations (23) – (27) are a system of *5J+5* equations for the solution of *5J+5* unknowns $f_j^n, u_j^n, v_j^n, s_j^n, t_j^n$, *j = 0, 1, 2 …, J*. This non-linear system of algebraic equations is *linearized* by means of Newton's method as explained in [44-47].

Phase d: Block-tridiagonal Elimination of Linear Keller Algebraic Equations

The linear system (23) – (27) can now be solved by the block-elimination method, since they possess a *block-tridiagonal* structure. Commonly, the block-tridiagonal structure consists of variables or constants, but in this case comprises *block matrices*. The complete linearized system is formulated as a *block matrix system*, where each element in the coefficient matrix is a matrix itself. Then, this system is solved using the second order accurate Keller-box method. The numerical results are affected by the number of mesh points in both directions. After some trials in the η-direction a larger number of mesh points are selected whereas in the ξ direction (tangential coordinate) significantly less mesh points are utilized. η_{max} has been set at 8 and this defines an adequately large infinity boundary condition required to achieve smooth solutions. ξ_{max} is set at

1.0 for this flow domain. Mesh independence is therefore achieved in the present computations. The computer program of the algorithm is executed in **MATLAB** running on a PC. The method demonstrates excellent stability, convergence and consistency, as elaborated by Keller [44].

4. NUMERICAL RESULTS AND INTERPRETATION

In order to verify the accuracy of the Keller- box solutions, computations are benchmarked with earlier results reported by Alam *et al.* [48] results as shown in **Table 1**. With $\beta \to \infty$, the present model reduces to the Newtonian model considered by Alam *et al.* [48]. The values of the skin friction and heat transfer coefficients are shown in Table1 for different values of ξ**.** Evidently skin-friction coefficient *decreases* with increasing values of ξ and the local heat transfer coefficient *conversely increases* with the increasing values of ξ**.** Very close correlation is achieved between the Keller-box computational results and the solutions of Alam *et al*. [48]. Confidence in the Keller-box numerical code is therefore justifiably high. **Table 2** indicates that skin-friction decreases for different values of S_f, S_T and *Pr*. In other words, increasing momentum and thermal slip significantly decelerate the flow as does a decrease in thermal conductivity of the polymer (Prandtl number is inversely proportional to thermal conductivity). However, the influence of the slip parameters on skin friction is more impactful. With increase in ξ values i.e. as we move along the cone periphery away from the apex, buoyancy forces are enhanced. This generates a strong decrease in skin friction (deceleration) and an enhancement in heat transfer rate i.e. Nusselt number function. **Table 3** presents the influence of $S_f, S_T, \Pr \text{ and } \beta$ on the wall heat transfer rate i.e. Nusselt number, $-\theta'(\xi,0)$. An increase in hydrodynamic slip (S_f), thermal slip (S_T) and Casson parameter (β) induces a substantial decrease in the magnitude of $-\theta'(\xi,0)$.

Table 1. Numerical values of skin-friction and heat transfer coefficient for different values of ξ while *Pr =0.71, S_f =0.5 and S_T =1.0* when $\beta \to \infty$ *(Newtonian case).*

ξ	Alam *et.al* results [48]		Present results	
	$f''(\xi,0)$	$-\theta'(\xi,0)$	$f''(\xi,0)$	$-\theta'(\xi,0)$
0.0	0.891936	0.420508	0.892157	0.421782
0.5	0.896407	0.620748	0.897843	0.619852
1.0	0.856963	0.848082	0.848784	0.840231
1.5	0.779210	1.129365	0.771562	1.119786
2.0	0.674111	1.441742	0.675320	1.432852
3.0	0.434152	2.202662	0.412372	2.063725

Table 2. Skin-friction coefficient $\left(1+\frac{1}{\beta}\right) f''(0)$ for different values of S_f, S_T and Pr with $\beta = 1.0$

S_f	S_T	Pr	$-\left(1+\frac{1}{\beta}\right) f''(0)$
0.0	1.0	0.7	0.7897
0.6			0.5591
1.0			0.3862
1.2			0.2943
0.5	0.0		0.8136
	0.5		0.7087
	1.0		0.5999
	2.0		0.3662
	1.0	0.001	0.9684
		0.1	0.9577
		0.71	0.5999
		1.0	0.5446

Table 3: Values of Nusselt number i.e. $-\theta'(0)$ for different values of S_f, S_T, Pr and β **.**

S_f	S_T	Pr	β	$-\theta'(0)$
0.0	1.0	0.71	1.0	0.3523
0.5				0.3098
1.0				0.2656
0.5	0.0			0.4619
	0.5			0.3845
	1.0			0.3098
	1.0	0.01		0.1074
		0.1		0.1505
		0.71		0.3095
		0.71	0.5	0.3215
			1.4	0.3091
			2.0	0.3090

The contrary response is computed with an increase in Prandtl number (*Pr*). With increasing β values, less heat is transferred from the boundary layer regime to the cone surface (the fluid is heated and the cone surface is cooled). This manifests in a decrease in Nusselt numbers with greater viscoplastic effect (*larger β values).* Similar observations have been reported by for example Mustafa *et al*. [16]. With increasing Prandtl number, thermal diffusivity is reduced and thermal conductivity is increased. This decreases temperatures in the boundary layer and enhances heat transfer rates to the cone surface i.e. boosts Nusselt numbers.

Figs 2- 9 present velocity and temperature distributions for variations in specific key thermo physical parameters, namely hydrodynamic slip (S_f), thermal slip (S_T), Casson parameter

(β) and Prandtl number (Pr). In all graphs ξ is constrained as unity and S = 0.5 (wall suction). **Fig. 2** exhibits the effect of velocity slip parameter, S_f on the velocity. It is seen apparent that the flow is markedly decelerated in the vicinity of the cone surface with greater wall momentum slip. Velocity peaks some distance from the wall and thereafter momentum slip induces a notable acceleration in the flow i.e. decreases momentum boundary layer thickness. The slip effect is therefore opposing near the cone surface and assistive further into the boundary layer transverse to the cone surface. Greater momentum slip retards the fluid motion near and at the upper wall. Moreover, dragging of the fluid adjacent to the cone surface is partially transmitted into the fluid partially which induces a deceleration near the wall; however this is eliminated and reversed further from the cone surface. The peak velocity is observed to migrate with greater momentum slip further from the cone surface. The inhibitive nature of slip close to the boundary and beneficial effect further from the boundary has also been confirmed in many other studies including Saleem and Nadeem [37]. In all profiles, a smooth decay is observed into the free stream demonstrating excellent convergence of the numerical solution and the imposition of an adequately large infinity boundary condition.

Fig.3 presents the evolution in temperature function, $\theta(\eta)$, with transverse coordinate η with variation in hydrodynamic slip parameter, S_f. Temperature profiles consistently decay monotonically from a maximum at the cone surface to the free stream. All profiles converge at a large value of transverse coordinate, again showing that a sufficiently large infinity boundary condition has been utilized in the numerical computations. Greater momentum slip substantially increases temperatures in the boundary layer and therefore also elevates thermal boundary layer thickness. The regime is therefore coolest when slip is absent (S_f =0 i.e. *no-slip classical case*) and hottest with strong hydrodynamic wall slip.

Figs. 4 and 5 illustrate the influence of thermal slip parameter (S_T) on the velocity and temperature. Both velocity and temperature are consistently suppressed with an increase in S_T. Temperatures are strongly depressed in particular at the cone surface. Greater thermal jump therefore decelerates the flow and cools the boundary layer. Momentum boundary layer thickness is enhanced whereas thermal boundary layer thickness is decreased with increasing thermal slip. A similar response has been observed by Basir *et al.* [49]. Physically, as the thermal slip parameter rises, the fluid flow within the boundary layer becomes progressively less sensitive to the heating effects at the cone surface and a decreased quantity of thermal energy (heat) is transferred from

the hot cone surface to the fluid, resulting in a fall in temperatures, manifesting in a cooling and thinning of the thermal boundary layer. This has important implications in thermal polymer enrobing, since thermal slip modifies the heat transferred to the polymer material which in turn alters characteristics of the final product as explained by Dealy and Wissbrun [42].

Figs. 6 and 7, depict the effect of Casson fluid parameter, β on velocity and temperature profiles. It is shown that the effect of β *enhances velocity near the cone surface* but *depletes* it further away. Increasing Casson parameter however consistently *weakly* decreases temperatures throughout the boundary layer. The influence on velocity field is significantly greater however since the viscoplastic effect is simulated solely in the momentum equation (7) via the shear term $\left(1+\frac{1}{\beta}\right)f'''$ and in the velocity boundary condition at the cone surface in eqn. (9), i.e. $f'(0)=\left(1+\frac{1}{\beta}\right)S_f\, f''(0)$. However via *coupling* of the energy eqn. (8) and momentum equation (free convection), the effect of viscoplastic parameter is indirectly transmitted to the temperature field. Since the Casson parameter is also present in the wall boundary condition, the acceleration effect is only confined to the region close to the cone surface. Further from this zone, the velocity slip factor, S_f will exert a progressively reduced effect and an increase in Casson parameter, β, will manifest with a deceleration in the flow. Overall however the dominant influence of β, is near the wall and is found to be assistive to momentum development. Only a very small decrease in temperature is observed with a large enhancement in Casson fluid parameter as shown in Fig. 7.

Figs. 8 - 9, present the impact of Prandtl number (*Pr*) on the velocity and temperature profiles along the transverse coordinate i.e. normal to the cone surface. Prandtl number epitomizes the ratio of momentum diffusion to thermal diffusion in the boundary layer regime. It also represents the ratio of the product of specific heat capacity and dynamic viscosity, to the fluid thermal conductivity. For *Pr equal to unity* both the momentum and thermal diffusion rates are the same, as are the momentum and thermal boundary layer thicknesses. An increment in *Pr* from 0.01 through 0.1, 0.3, 0.5, 0.7 to 1.0, which corresponds to increasing momentum diffusivity and decreasing thermal diffusivity, results in a tangible reduction in velocity magnitudes throughout the boundary layer. For *Pr <1*, thermal diffusivity surpasses momentum diffusivity i.e. heat will diffuse at a faster rate than momentum. In this manner for lower Pr fluids (e.g. *Pr = 0.01* which physically relate to liquid metals), the flow will be accelerated whereas for greater Pr fluids (e.g.

Pr = 1 for low weight molecular polymers [42]) it will be strongly decelerated, as observed in Fig.9. For *Pr < 1*, the momentum boundary layer thickness is lesser than thermal boundary layer thickness.

5. CONCLUSIONS

A theoretical study has been conducted of laminar incompressible free convection boundary layer flow of a viscoplastic (Casson) fluid from a vertical non-isothermal cone. Momentum and thermal slip effects have been incorporated in the model. The transformed boundary layer equations for heat and momentum conservation have been solved using a finite difference method for the case of suction present at the cone surface. Verification of the accuracy of the Keller - box computational code has been achieved via comparison with previous Newtonian solutions reported in the literature. The present investigation has shown that:

1) Increasing the velocity slip parameter (S_f) reduces the velocity near the cone surface and increases the temperature i.e. enhances momentum boundary layer thickness and decreases thermal boundary layer thickness. However flow reversal is never computed.

2) Increasing thermal slip parameter, (S_T) consistently decelerates the flow and also decreases temperature (and thermal boundary layer thickness).

3) Increasing Casson viscoplastic fluid parameter (β), increases the velocity near the cone surface but decreases velocity further from the cone, and also fractionally lowers the temperature throughout the boundary layer regime i.e. reduces thermal boundary layer thickness.

4) Increasing Prandtl number (*Pr*) decelerates the flow and also strongly depresses temperatures, throughout the boundary layer regime.

The present study has neglected *time-dependent* and *mass transfer (species diffusion)* effects, which are also important in polymer processing and these will be examined in the future.

Acknowledgements:

The authors are grateful to the reviewers for giving their constructive comments for improving this article. The work is supported by the University Grants Commission-SERO - Ref. No. MRP 4613/14. The corresponding author is thankful to UGC-SERO and management of MITS, Madanapalle.

REFERENCES

[1] S. Livescu, Mathematical modeling of thixotropic drilling mud and crude oil flow in wells and pipelines—A review, *J. Petroleum Science and Engineering*, 98/99, 174–184 (2012).

[2] J. Hron, J. Málek, P. Pustějovská and K. R. Rajagopal, On the modeling of the synovial fluid, *Advances in Tribology*, Volume 2010 (2010), Article ID 104957, 12 pages. http://dx.doi.org/10.1155/2010/104957.

[3] F. Loix, L. Orgéas, C. Geindreau, P. Badel, P. Boisse and J.-F. Bloch, Flow of non-Newtonian liquid polymers through deformed composites reinforcements, *Composites Science and Technology*, 69, 612–619 (2009).

[4] Viviane Kechichian, Gabriel P. Crivellari, Jorge A.W. Gut, Carmen C. Tadini, Modeling of continuous thermal processing of a non-Newtonian liquid food under diffusive laminar flow in a tubular system, *Int. J. Heat and Mass Transfer*, 55, 5783–5792 (2012).

[5] M. Ghannam, N. Esmail, Flow behavior of enhanced oil recovery alcoflood polymers, *J. Applied Polymer Science*, 85 (14): 2896 - 2904 (2002).

[6] N. Casson, A flow equation for pigment oil-suspensions of the printing ink type, *Rheology of Disperse Systems (C.C. Mill, ed.)*, pp. 84. Pergamon Press, London (1959).

[7] R. B. Bird, G. C. Dai and B. J. Yarusso, The rheology and flow of viscoplastic materials, *Rev. Chem. Eng*, 1, 1-83 (1983).

[8] T. Hayat, I. Pop and A. A. Hendi, Stagnation-point flow and heat transfer of a Casson fluid towards a stretching sheet, *Zeitschrift fur Naturforschung*, 67, 70-76 (2012).

[9] M. S. Nasir, A. S. Butt and A. Ali, Unsteady chemically-reacting Casson fluid flow in an irregular channel with convective boundary, *Zeitschrift fur Naturforschung A*,70 (8) 10-18 (2015).

[10] Ch. R. Reddy, Ch. Venkata Rao, O. Surender, Soret, Joule heating and Hall effects on free convection in a Casson fluid saturated porous medium in a vertical channel in the presence of viscous dissipation, *Proc. Engineering*, 127, 1219-1226 (2015).

[11] P. Nagarani and A. Lewis, Peristaltic flow of a Casson fluid in an annulus, *Korea Australia Rheology J.*, 24, 1–9 (2012).

[12] T. V. Pham and E. Mitsoulw, Entry and exit flows of Casson fluids, *Canadian J. Chemical Engineering*, 72, 1080-1084 (1994).

[13] D. Tripathi and O.Anwar Bég, Mathematical modeling of peristaltic propulsion of viscoplastic fluids, *Proc. IMECHE- Part H; J. Engineering in Medicine*, 228 (1): 67-88 (2014).

[14] Hao Xiang and Bin Chen, Simulating non-Newtonian flows with the moving particle semi-implicit method with an SPH kernel, *Fluid Dynamics Research*, 47, 015511 (2015).

[15] R. A. Shankaran, Numerical simulation of flow of shear-thinning fluids in corrugated channels, *MSc Thesis, Mechanical Engineering, Texas A&M University*, USA, December (2007).

[16] M. Mustafa, T. Hayat, I. Pop and A. Aziz, Unsteady boundary layer flow of a Casson fluid due to an impulsively started moving flat plate, *Heat Transfer-Asian Research*, 40, 563–576 (2011).

[17] R L Batra and Bigyani Das, Flow of a Casson fluid between two rotating cylinders, *Fluid Dynamics Research*, 9, 133 (1992).

[18] N. S. Akbar, D. Tripathi, O. Anwar Bég, Z. H. Khan, MHD dissipative flow and heat transfer of Casson fluids due to metachronal wave propulsion of beating cilia with thermal and velocity slip effects under an oblique magnetic field, *Acta Astronautica* (2016). In press

[19] W.B. Black, Wall slip and boundary effects in polymer shear flows, *PhD Thesis, Chemical Engineering, University of Wisconsin – Madison, USA* (2000).

[20] S.-Q. Wang, P. A. Drda, and Y.-W. Inn, Exploring molecular origins of sharkskin, partial slip, and slope change in flow curves of linear low density polyethylene, *J. Rheology*, 40(5):875–898 (1996).

[21] J.-M. Piau, N. E. Kissi, F. Toussaint, and A. Mezghani, Distortions of polymer extrudates and their elimination using slippery surfaces, *Rheol. Acta*, 34:40–57 (1995).

[22] J. M. Piau and N. E. Kissi, Measurement and modelling of friction in polymer melts during macroscopic slip at the wall, *J. Non-Newtonian Fluid Mech*., 54:121–142 (1994).

[23] F. J. Lim and W. R. Schowalter, Wall slip of narrow molecular weight distribution polybutadienes, J. Rheology, 33(8):1359–1382 (1989).

[24] S. G. Hatzikiriakos and N. Kalogerakis, A dynamic slip velocity model for molten polymers based on a network kinetic theory, *Rheol. Acta*, 33:38–47 (1994).

[25] Y. Liu and M. Gehde, Effects of surface roughness and processing parameters on heat transfer coefficient between polymer and cavity wall during injection molding, *The Int. J. Advanced Manufacturing Technology*, 84, 1325-1333 (2016).

[26] Savvas G Hatzikiriakos and Evan Mitsoulis, Slip effects in tapered dies, *Polymer Engineering and Science*, 49(10):1960 - 1969 (2009).

[27] E.M. Sparrow, S.H. Lin, Laminar heat transfer in tubes under slip-flow conditions, *ASME J. Heat Transfer*, 84, 363-639 (1962).

[28] A. Subba Rao, Ramachandra Prasad, V., Bhaskar Reddy, N. and Anwar Bég, O., Heat transfer in a Casson rheological fluid from a semi-infinite vertical plate with partial slip. *Heat Trans. Asian Res*. 44 (3), 272-291 (2015).

[29] Md. Jashim Uddin, W.A. Khan, A.I.Md. Ismail and, O. Anwar Bég, Computational study of three-dimensional stagnation point nanofluid bio-convection flow on a moving surface with anisotropic slip and thermal jump effects, *ASME J. Heat Transfer* (2016). DOI: 10.1115/1.4033581 (8 pages).

[30] Subba Rao, V.R.Prasad, K. Harshavalli and O. Anwar Bég, Thermal radiation effects on non-Newtonian fluid in a variable porosity regime with partial slip, *J. Porous Media*, 19 (4): 313–329 (2016).

[31] R.G. Hering, R. J. Grosh, Laminar free convection from a non-isothermal cone, *Int. J. Heat Mass Transfer*, 5(11), 1059–1068 (1962).

[32] R.G. Hering, Laminar free convection from a non-isothermal cone at low Prandtl numbers, *Int. J. Heat Mass Transfer*, 8(10), 1333–1337 (1965).

[33] M. Alamgir, Overall heat transfer from vertical cones in laminar free convection- an approximate method, *ASME J. Heat Transfer*, 101(1–4), 174–176 (1979).

[34] M.A. Hossain, S.C. Paul, Free convection from a vertical permeable circular cone with nonuniform surface temperature, *Acta Mechanica*, 151(1–2), 103–114 (2001).

[35] A.J. Chamkha, Coupled heat/mass transfer by natural convection about a truncated cone in the presence of magnetic field and radiation effects, *Num. Heat Transfer: A*, 39, 511-530 (2001).

[36] O. Anwar Bég, J. Zueco, Tasveer A. Bég, A. Kadir and U.F. Khan, Network electro-thermal simulation of non-isothermal magnetohydrodynamic heat transfer from a transpiring cone with pressure work effects, *Int. J. Applied Computational Mathematics* (2016).

[37] S. Saleem and S. Nadeem, Theoretical analysis of slip flow on a rotating cone with viscous dissipation effects, *J. Hydrodynamics* (2015). DOI: 10.1016/S1001-6058(15)60523-6

[38] O. Anwar Bég, M.J. Uddin, T. Bég, R. Reddy Gorla, Numerical simulation of self-similar thermal convection from a spinning cone in anisotropic porous medium, *J. Hydrodynamics Series B,* 28 (2):184-194 (2016).

[39] Md Faisal Md Basir, M.J. Uddin, A. I. Md. Ismail and O. Anwar Bég, Unsteady bio-nanofluid slip flow over a stretching cylinder with bioconvection Schmidt and Péclet number effects, *AIP Advances*, 6, 055316-1 - 055316-15 (2016).

[40] V. R. Prasad, A. S. Rao, N. B. Reddy, and O. Anwar Bég, Modelling laminar transport in a Casson fluid from an isothermal sphere with partial slip in a non-Darcy porous medium, *Theoretical and Applied Mechanics*, 40 (4), 469-510 (2013).

[41] A. Subba Rao, V.R. Prasad, N. Bhaskar Reddy and O. Anwar Beg, Modelling laminar transport phenomena in a Casson rheological fluid from an isothermal sphere with partial slip; *Thermal Science*, 19, 1507-1519 (2015).

[42] J. Dealy and K. Wissbrun, *Melt Rheology and its Role in Plastics Processing: Theory and Applications,* Van Nostrand Reinhold, New York (1990).

[43] K.A. Yih, Effect of blowing/suction on MHD-natural convection over horizontal cylinder: UWT or UHF, *Acta Mechanica*, 144, 17-27 (2000).

[44] T. Cebeci and P. Bradshaw, *Physical and Computational Aspects of Convective Heat Transfer*, *Springer*, *New York* (1984).

[45] H.B. Keller, A new difference method for parabolic problems, *J. Bramble (Editor), Numerical Methods for Partial Differential Equations, Academic Press, New York, USA* (1970).

[46] A. Subba Rao, N. Nagendra, and V.R. Prasad, Heat transfer in a non-Newtonian Jeffrey's fluid over a non-isothermal wedge, Procedia Engineering, Elsevier, vol. 127C, pp. 775-782 (2015)., Doi:10.1016/j.proeng.2015.11.412

[47] V. R. Prasad, S. A. Gaffar and O. Anwar Bég, Heat and mass transfer of a nanofluid from a horizontal cylinder to a micropolar fluid, *AIAA J. Thermophysics Heat Transfer*, 29, 1, 127-139 (2015).

[48] Md.M. Alam, M.A. Alim, Md.M.K. Chowdhury, Free convection from a vertical permeable circular cone with pressure work and non-uniform surface temperature, *Nonlinear Analysis: Modelling and Control*, 12, 21–32 (2007).

FIGURE CAPTIONS:

Fig 1(a): Physical Model and Coordinate System

Fig 1(b): Grid meshing and a "Keller Box" computational cell

Fig.2. Influence of S_f on velocity profiles

Fig.3. Influence of S_f on temperature profiles

Fig.4. Influence of S_T on velocity profiles

Fig.5. Influence of S_T on temperature profiles

Fig.6. Influence of β on velocity profiles.

Fig.7. Influence of β on temperature profiles.

Fig.8. Influence of Pr on velocity profiles

Fig.9. Influence of Pr on temperature profiles

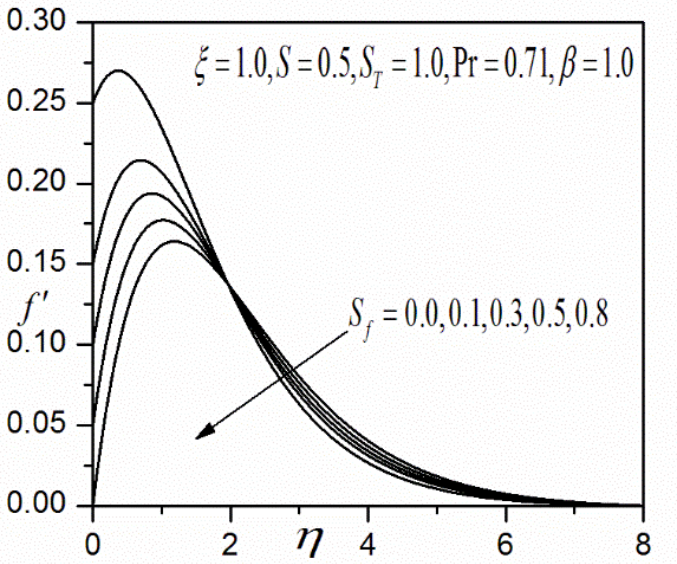

Fig.2 Influence of S_f on the velocity.

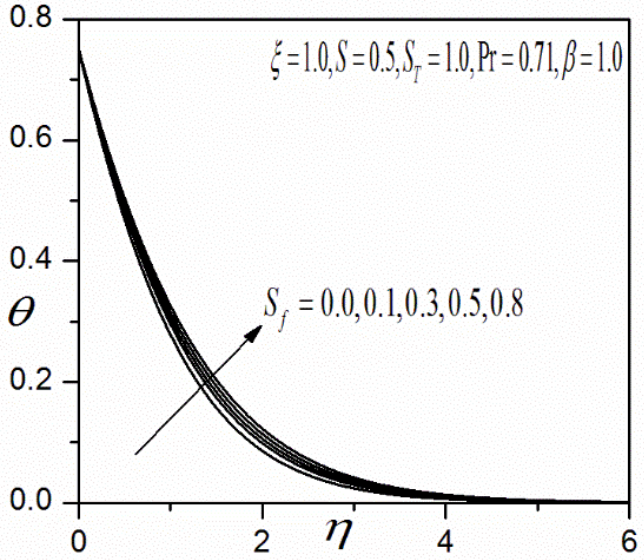

Fig.3 Influence of S_f on the temperature.

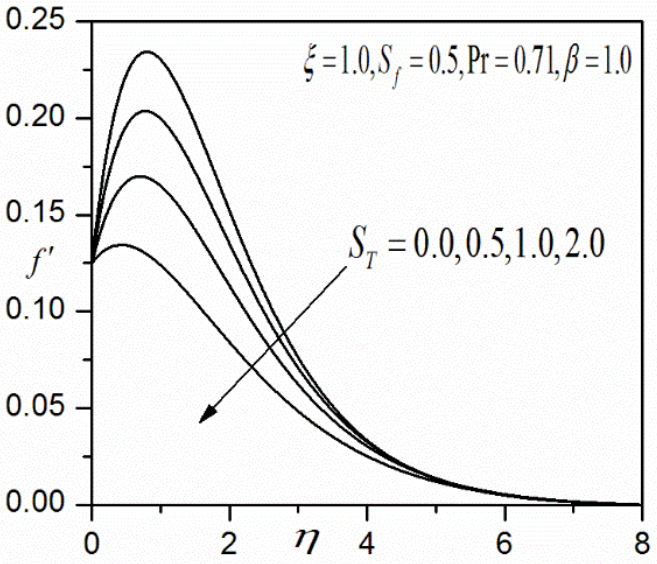

Fig.4 Influence of S_T on the velocity.

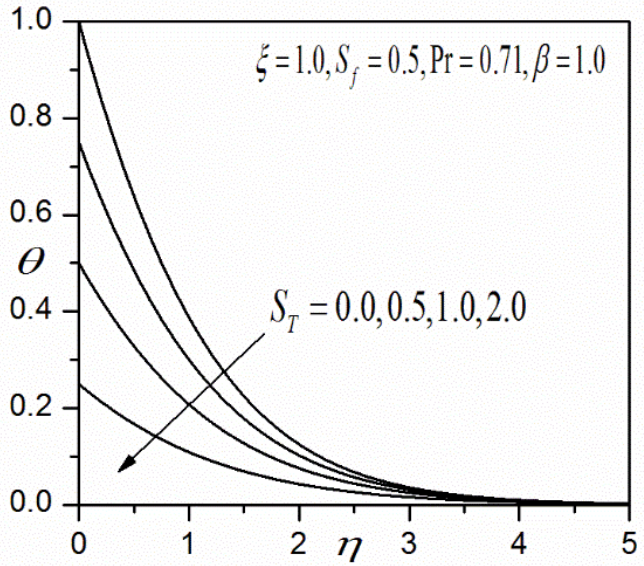

Fig.5 Influence of S_T on the temperature.

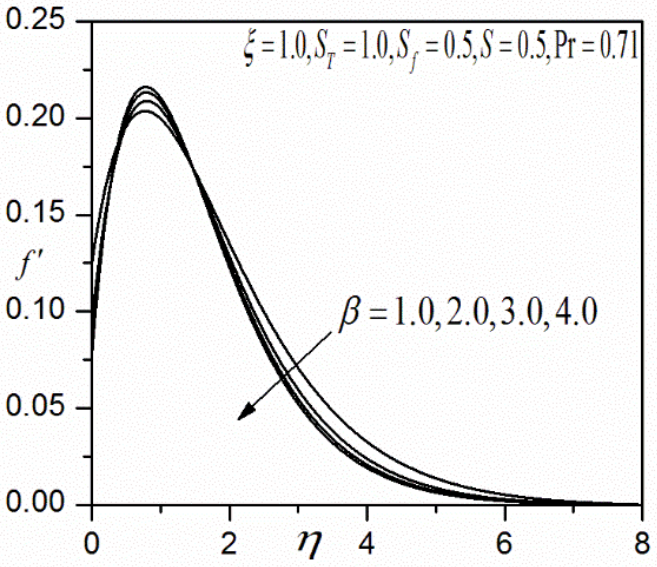

Fig.6 Influence of β on the velocity.

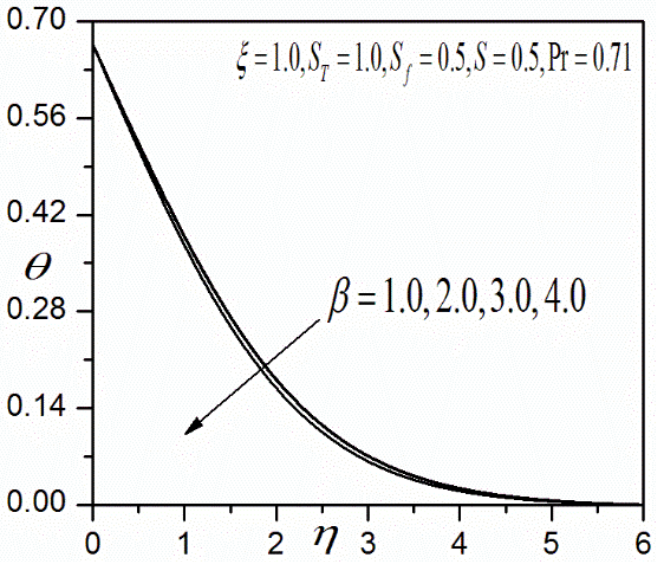

Fig.7 Influence of β on the temperature.

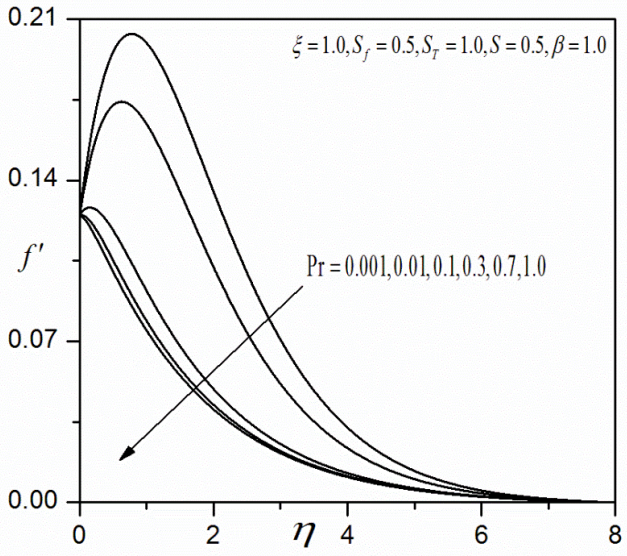

Fig.8 Influence of Pr on the velocity.

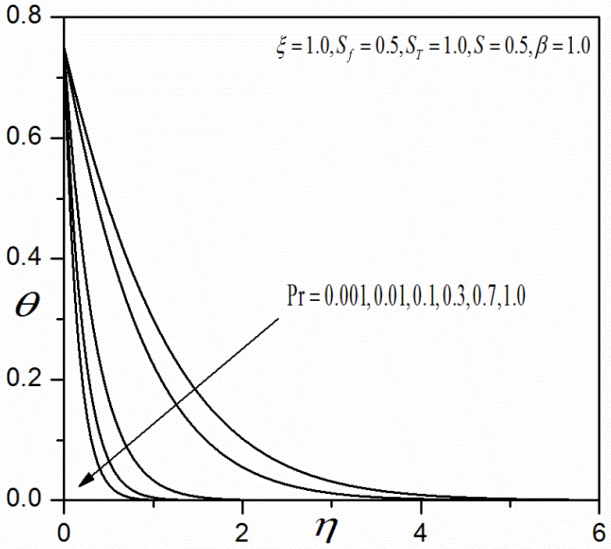

Fig.9 Influence of Pr on the temperature.